PHOTOCONDUCTIVITY AS A PROBE OF SEMICONDUCTING AND COLLECTIVE STATES IN THE LAYERED QUASI ONE-DIMENSIONAL COMPOUND TiS_3

***I.G. Gorlova*, S.A. Nikonov, S. G. Zybtsev and V. Ya. Pokrovskii**

Kotel'nikov Institute of Radioengineering and Electronics of RAS, Russia
E-mail: gorl@cplire.ru

ECRYS 2022

Crystal structure of TiS_3 whiskers

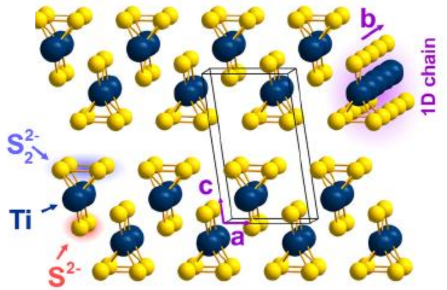

Unit cell parameters:
***a* = 0.50 nm, *b* = 0.34 nm, *c* = 0.88 nm.**
β = 98,4°
Structural type – monoclinic
Space group – P21/m
S. K. Srivastava and B. N. Avasthi,
J. of Materials Science, 27, 3693 (1992).

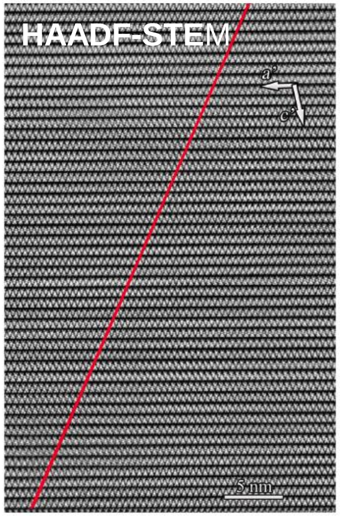

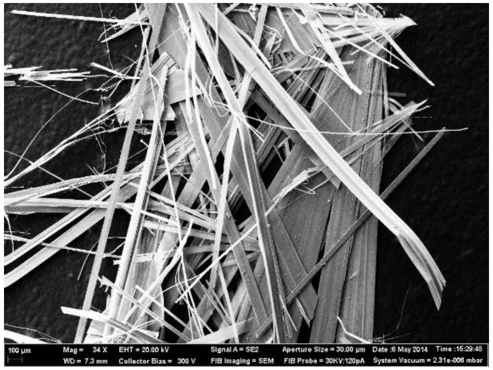

TiS_3 single crystal whiskers grown by **A.N. Titov** at Institute of Metal Physics, UB RAS, Yekaterinburg, Russia

.

A

B

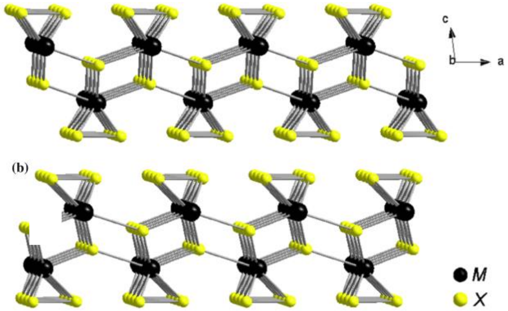

A- and B-variants of the MX_3 crystal structure (M = Ti, Zr, Hf; X = S, Se, Te).

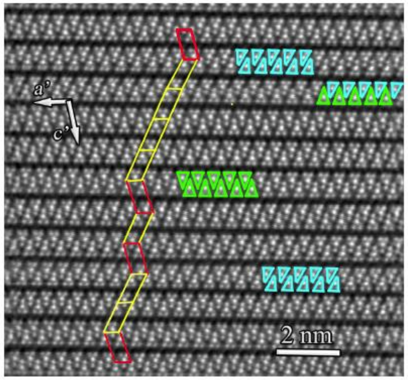

Structural defects: S vacancies, twins and B-variant fragments (blue triangles)

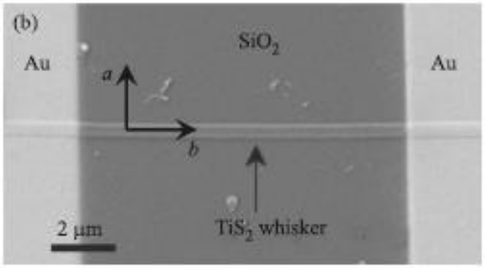

TiS_3 whisker with electrical Au contacts.

*I.N. Trunkin, I.G. Gorlova, N.B. Bolotina, V.I. Bondarenko, Y.M. Chesnokov, A.L. Vasiliev, J. Mater. Sci. **56**, 2150 (2021)*

Electronic band structure for TiS_3 at 300 K

TiS_3 is anisotropic n-type semiconductor with an optical band-gap $\boldsymbol{E_g} \approx$ **1 eV**

A donor energy level is found near E_F.

First principle investigation

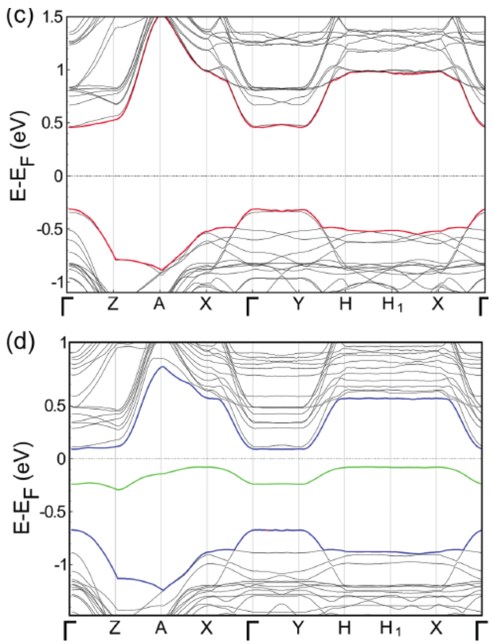

c) Electronic band structure for the clean TiS_3 system. d) Electronic band structure for the doped TiS_3 with sulphur vacancies (2%).

J. O. Island, M. Barawi, R. Biele, A. Almazan, J. M. Clamagirand, J. R. Ares, C. Sanchez, H. S. J. van der Zant, J. V. Alvarez, R. D'Agosta, I. J. Ferrer, and A. Castellanos-Gomez, Adv. Mater. ***27****, 2595 (2015).*

ARPES

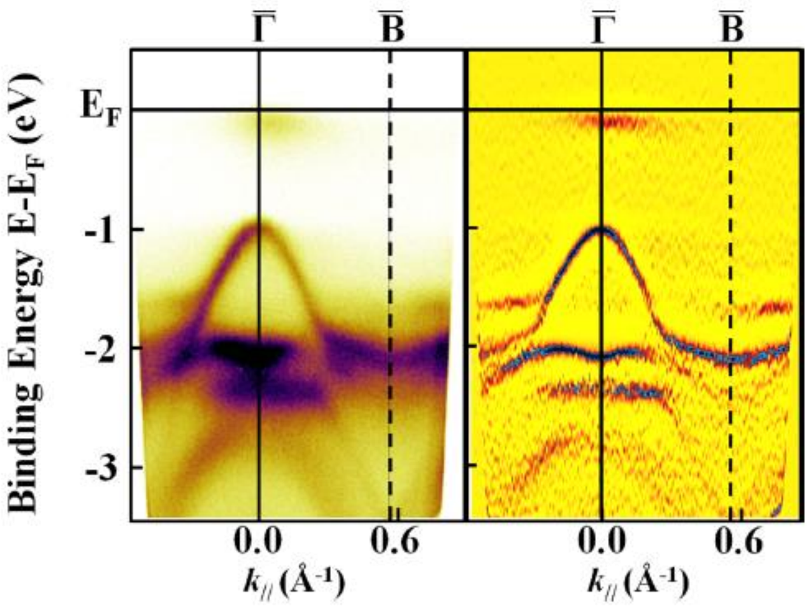

H. Yi, T. Komesu, S. Gilbert, G. Hao, A. Yost, A. Lipatov, A. Sinitskii, J. Avila, C. Chen, M. C. Asensio, and P. A. Dowben., Appl. Phys. Lett. ***112****, 052102 (2018).*

Temperature dependences of conductivity and thermo-electric power in TiS_3

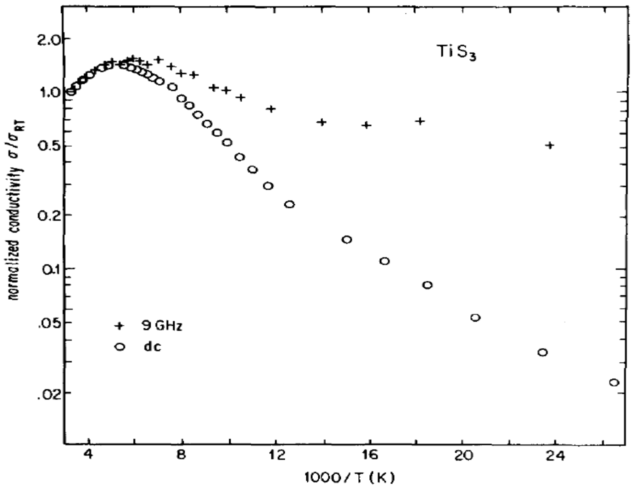

Fig. 1. Temperature dependence of the normalized dc and microwave conductivity in TiS_3.

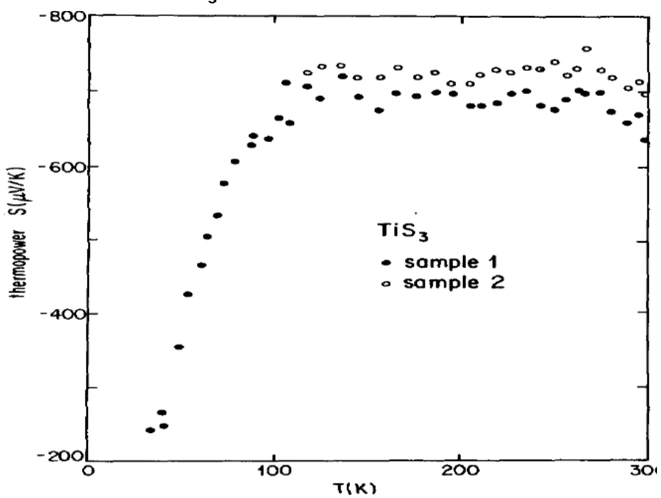

Fig. 2. Temperature dependence of the thermoelectric power in TiS_3.

Pei-Ling Hsieh, C. M. Jackson, and G. Grüner Solid State Commun., 46, 505 (1983).

Resistivity in the direction along the chains:

ρ_b(300 K) = 2.5 Ohm x cm.

Pei-Ling Hsieh, C. M. Jackson, and G. Grüner Solid State Commun., 46, 505 (1983).

ρ_b(300 K) = 0.2 Ohm x cm.

E. Finkman and B. Fisher, Solid State Commun 50, 25 (1984).

Electron density:

n(300 K)~2-5×10^{18} cm^{-3}.

O. Gorochov, A. Katty, N. Le Nagard, C. Levy-Clement, and D. M. Schleich, Mater. Res. Bull. 18, 111 (1983).

E. Finkman and B. Fisher, Solid State Commun 50, 25 (1984).

The anisotropy of conductivity of TiS_3 whiskers.

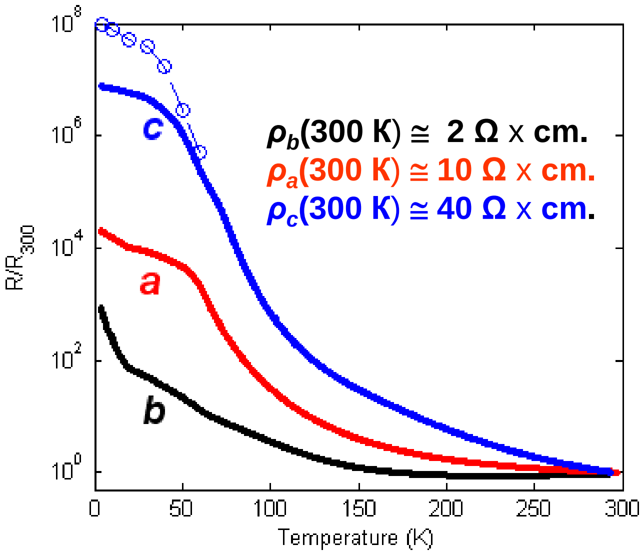

The temperature dependences of the resistance of TiS_3, measured along the ***a***, ***b***, and ***c*** axes

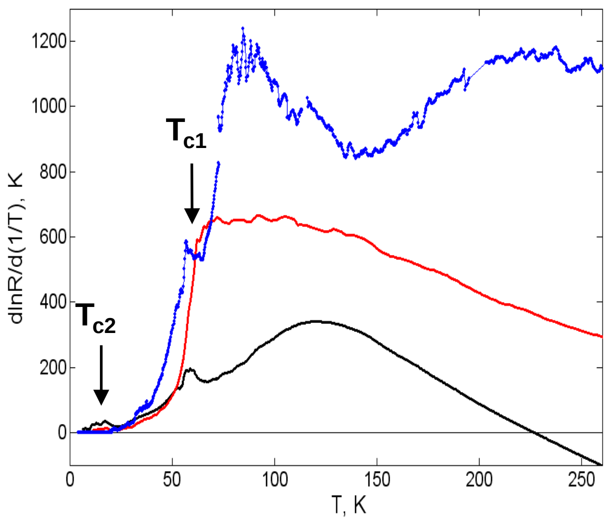

The temperature dependences of the logarithmic derivatives dln*R*/d(1/*T*) along the ***a***, ***b***, and ***c*** axes.

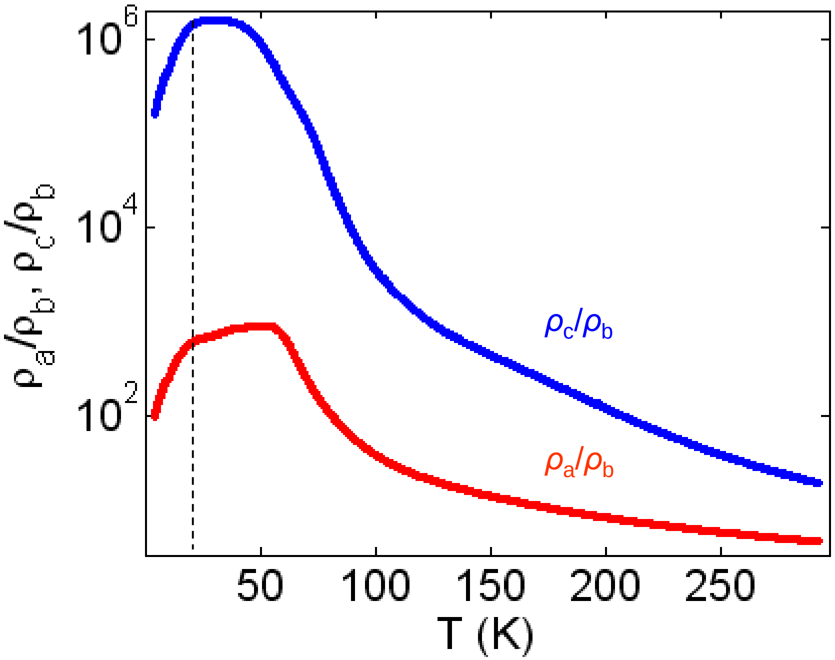

Temperature dependencies of the ratio ρ_a/ρ_b and ρ_c/ρ_b.

ρ_a/ρ_b ~ 5; ρ_c/ρ_b ~ 20 at 300 K.

ρ_c:ρ_a:ρ_b ~ 10^6:10^3:1 at T=50 K.

I.G. Gorlova S.G. Zybtsev and V.Ya. Pokrovskii, JETP Lett. ***100*** *256 (2014) .*

Nonlinear conductivity of TiS_3 whiskers.

$I \propto V^{\alpha(T)}$

In the *ab* plane

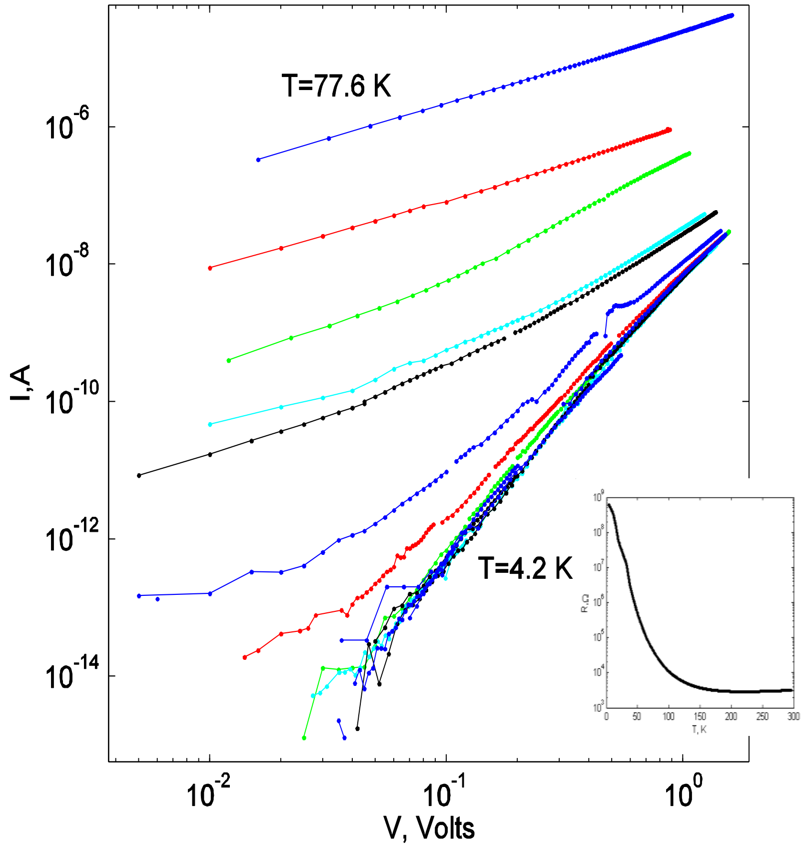

log *I*-log *V* curves measured along ***b*-axis** at *T* =4.2, 5.2, 5.6, 6.4, 7.7, 12.8, 24.7, 26.6, 41.5, 58.9, 77.6 K.
Inset: *R(T)* of the whiskers ρ_b(300 K) = 0.2 Ohm x cm.

Out-of-plane

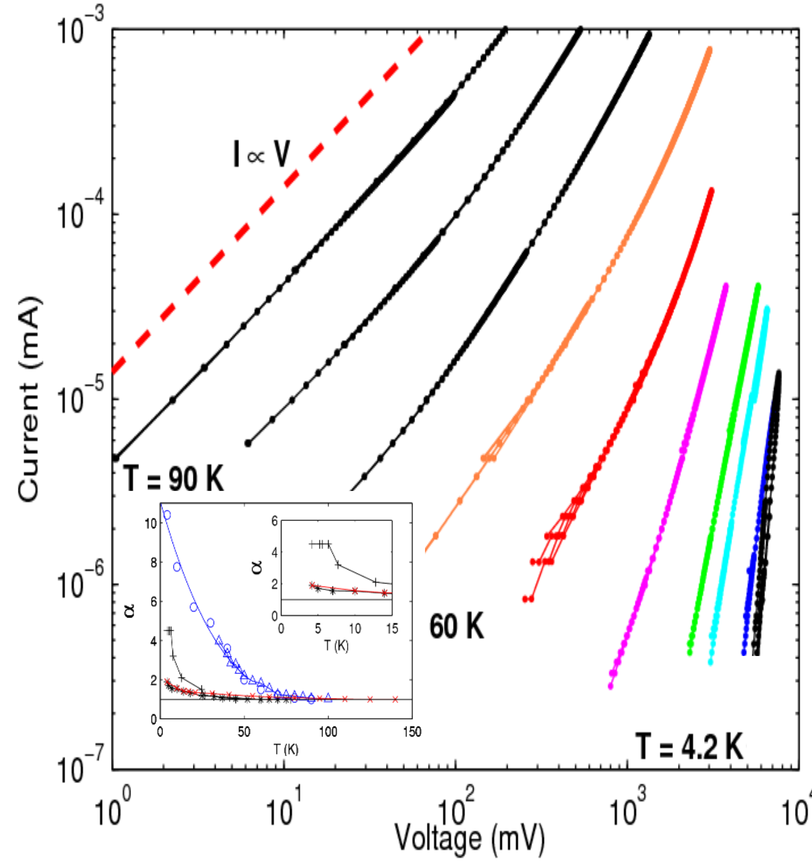

log *I*-log *V* curves measured along ***c*-axis** at *T* =4.2, 10, 20, 30, 40, 50, 60, 70, 80, 90 K
Inset: Temperature dependence of the exponent α(*T*) of the nonlinear *I*-*V* curves, $I \propto V^{\alpha(T)}$, along the ***a***, ***b***, and ***c*** axes.

I.G. Gorlova S.G. Zybtsev and V.Ya. Pokrovskii, JETP Lett. ***100*** *256 (2014) .*

Angle dependences of magnetoresistance of TiS_3

H* = 4x10^4 Oe, *I*||*b ***T<T$_{c1}$*** ***T≈T$_{c1}$*** ***T>T$_{c1}$***

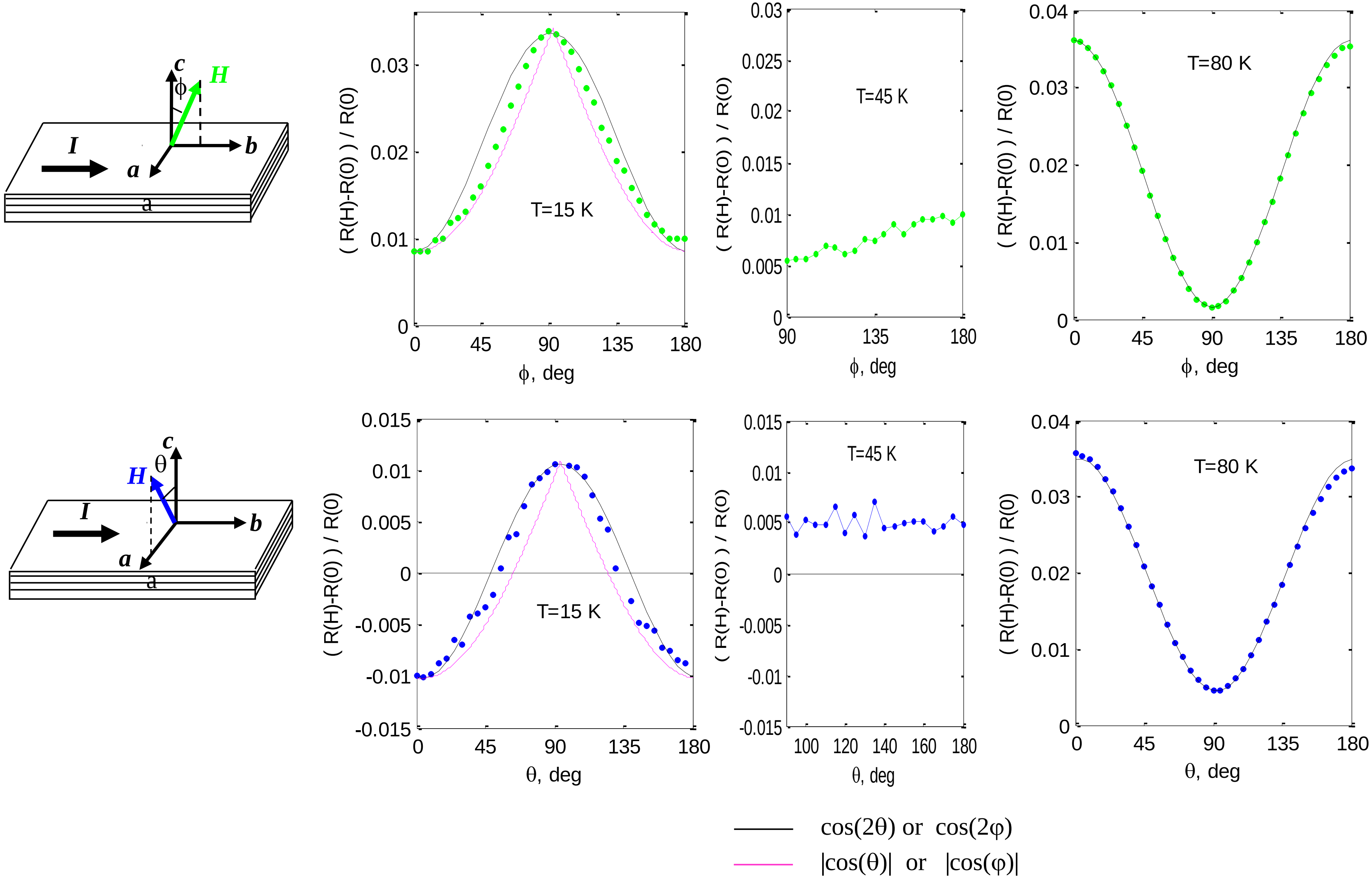

Temperature and field dependences of magnetoresistance for TiS_3

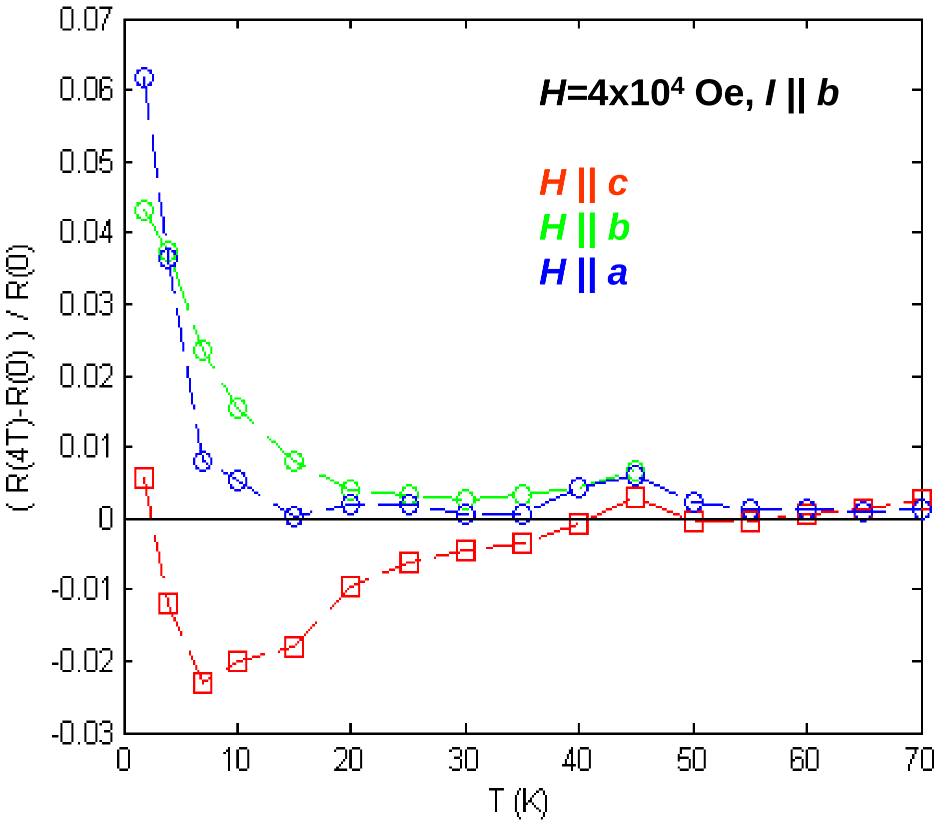

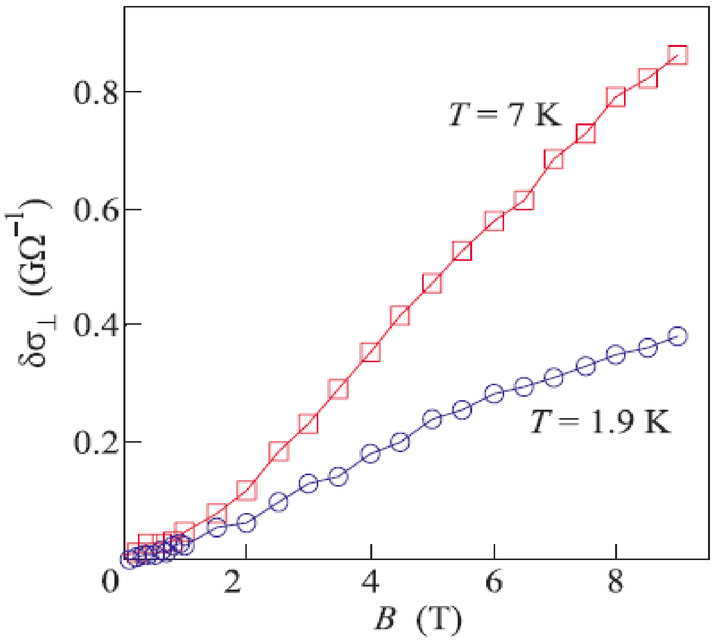

2D weak localization

$\Delta\sigma \sim B^2$, $B < 2T$

$\Delta\sigma \sim \log(B)$, $B > 2T$

I.G. Gorlova, V.Y. Pokrovskii, S.Y. Gavrilkin and A.Y. Tsvetkov, JETP Lett. ***107****, 175 (2018).*

Hall effect for TiS_3

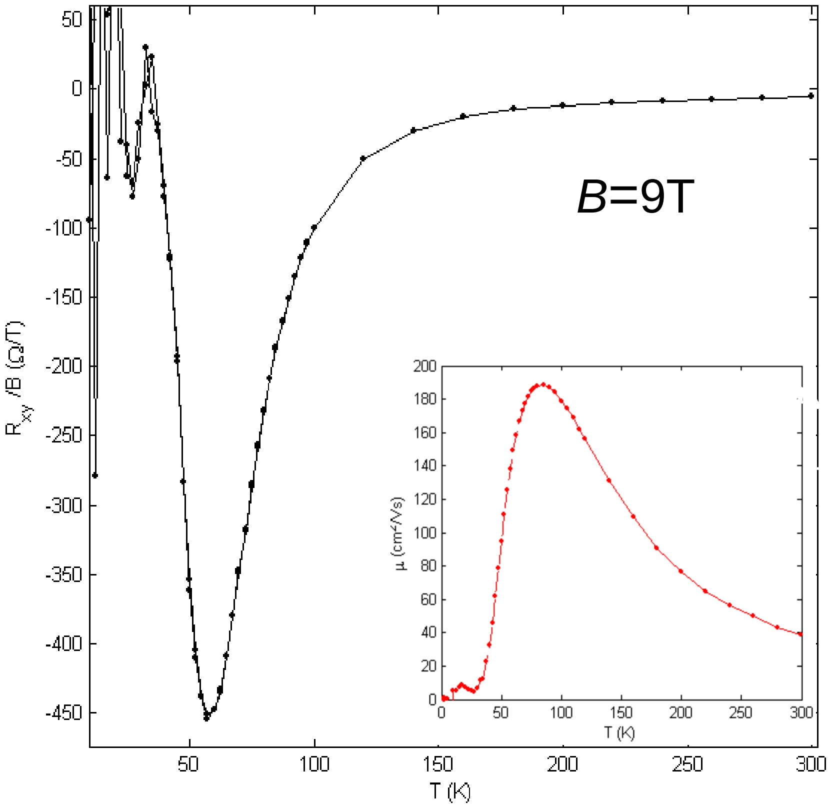

The temperature dependence of the Hall resistance for TiS_3 .
Inset: temperature dependence of the Hall mobility.
Electron density: n_{300}, ~10^{18} cm^{-3}, n_{50} ~10^{15} cm^{-3}.
Electron density per elementary conducting layer at 300 K is ~$10^{11}$$cm^{-2}$, at 50 K - ~ 5×$10^8$ cm^{-2}

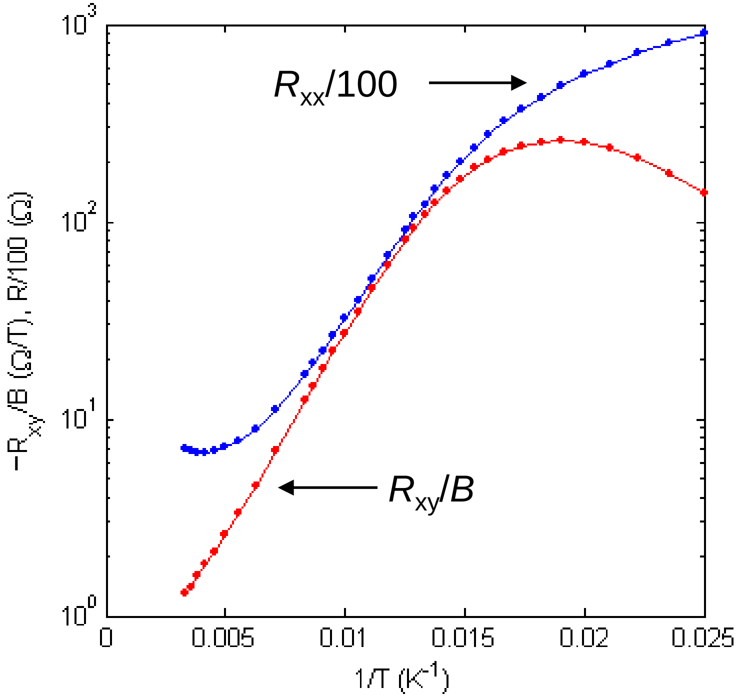

The temperature dependencies of the Hall resistance R_{xy} (B=9 T) and b-axis resistance R_{xx} for the same whisker.
The activation energy: for R_{xx}= 415 K, for R_{xy} = 469 K
.

*I.G. Gorlova, S.G. Zybtsev, V.Y. Pokrovskii, N.B. Bolotina, S.Y. Gavrilkin, A.Y. Tsvetkov, and A. N. Titov, Physica B **460** 11-15 (2015).*

Indications of a charge ordering phase transition in TiS_3

Power Law *I-V* curves in CDW compounds

TaS_3 –

*M.E. Itkis, F.Ya. Nad', P. Monceau, J. Phys.: Condens. Matter **2,** 8327 (1990).*

*S.K.Zhilinskii, M E Itkis, I.Yu. Kal'nova et.al., JETP **85**, 362 (1983).*

*S. V. Zaitsev-Zotov, Phys. Rev. Lett. **71**, 605 (1993).*

$NbSe_3$ –

*E. Slot et al., Phys. Rev. Lett. **95**, 176602 (2004)*

TaS_3

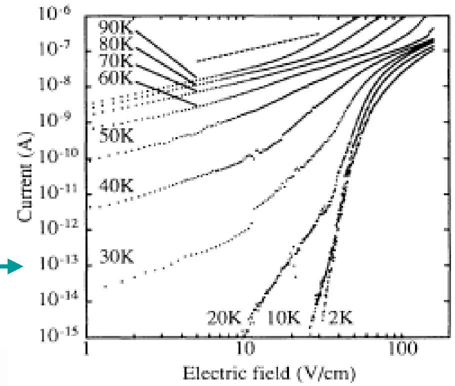

TiS_3

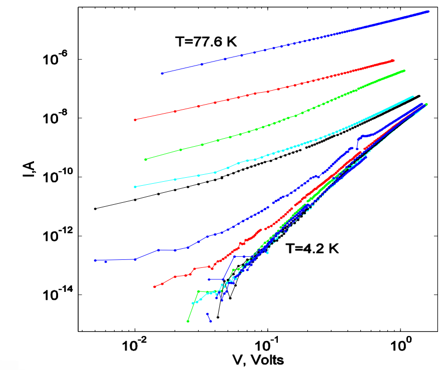

CDW sliding contribution to Hall effect in TaS_3 is opposite to that of quasiparticles.

*S.N. Artemenko, E.N. Dolgov, A.N. Kruglov, et al., JETP Lett. **39**, 258 (1984).*

Maximum of Hall effect at the Peierls transition temperature (63 K) for $ZrTe_3$

*S. Takahashi et al., Solid State Commun. **49** 1031 (1984).*

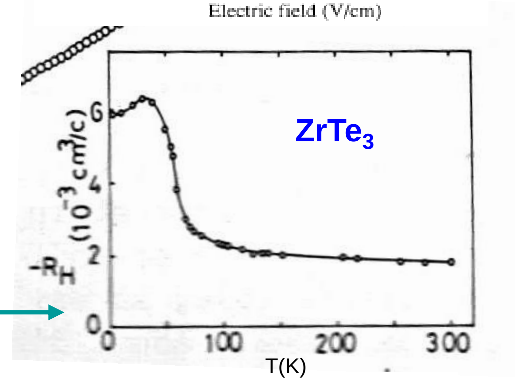

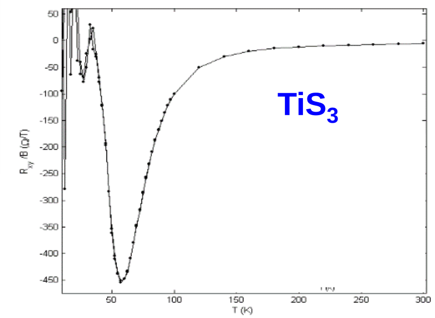

Negative magnetoresistance below ferroelectric CO phase transition temperature for α-$(BEDT\text{-}TTF)_2I_3$

*T. Ivek et al., Phys. Rev. B **96**, 075141 (2017).*

α-$(BEDT\text{-}TTF)_2I_3$

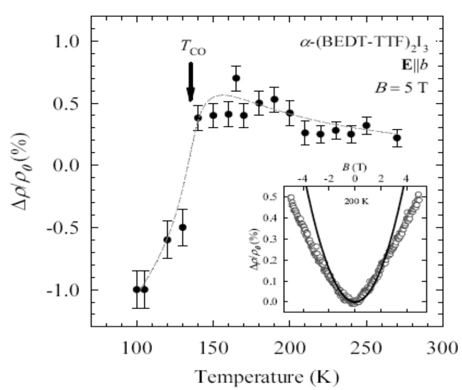

TiS_3

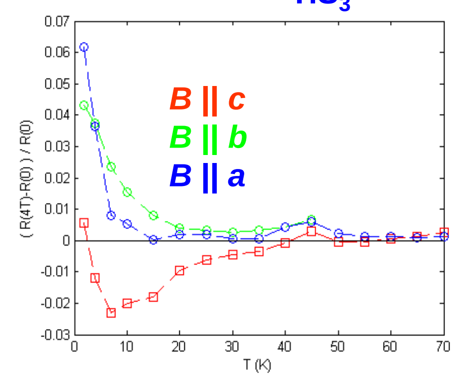

Field and Hall effects

TiS_3

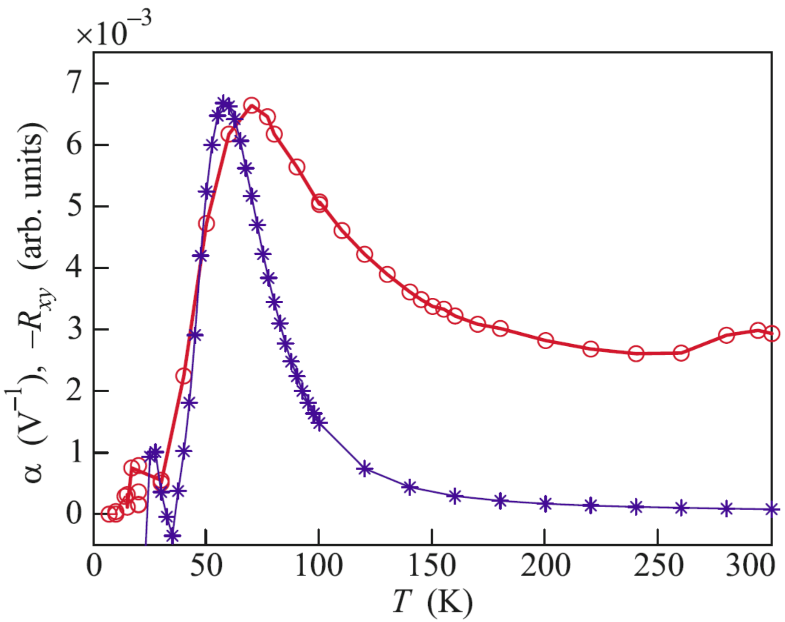

Temperature dependences of the gate-voltage sensitivity **$\alpha \equiv 1/\sigma\, d\sigma/dV_g$** (o) of the conductivity and the Hall resistance **$-R_{xy}$** (*) for the TiS_3 whiskers.

*I. G. Gorlova, A. V. Frolov, A. P. Orlov, V. Y. Pokrovskii, and W. W. Pai, JETP Lett. **110**, 417 (2019).*

CDW

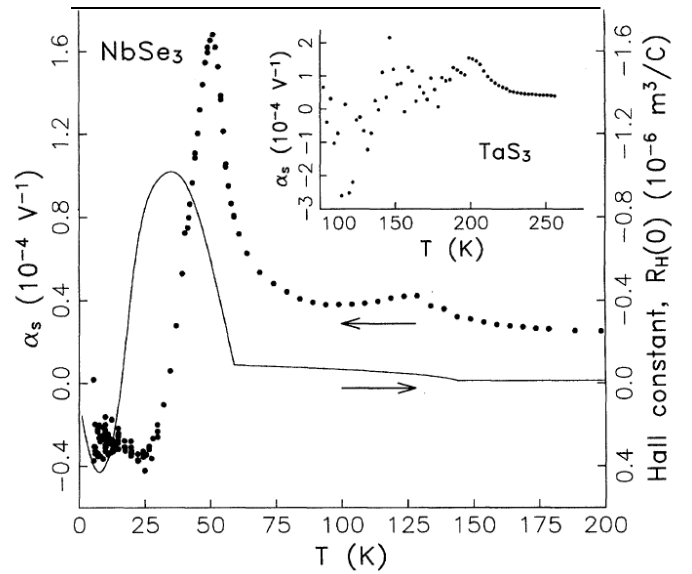

FIG. 4. Gate-voltage sensitivity $\alpha_s \equiv (1/R_s)\partial R_s/\partial V_G$ of the single-particle resistance R_s vs temperature for a 5.7×10^{-3} μm^2 $NbSe_3$ crystal. The temperature variation of the Hall constant $R_H(0)$ [6] is shown for comparison. The inset shows $\alpha_s(T)$ for a 5×10^{-3} μm^2 TaS_3 crystal.

*T.L. Adelman, S.V. Zaitsev-Zotov, and R.E. Thorne PRB **74** 5264 (1995)*

Photoconductivity at 300 K. TiS_3 nanoribbon photodetectors.

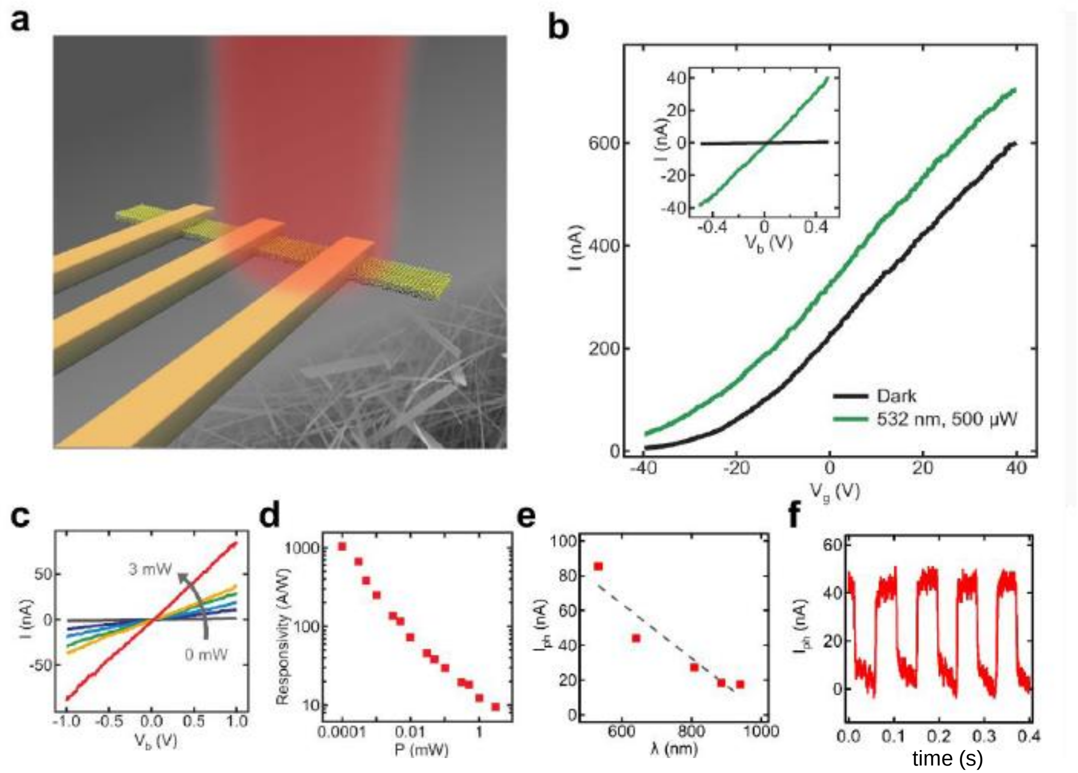

Photoresponsivity - 2910 A/W

Cutoff frequency ~ 1000Hz

Figure 9. (a) Model representation of a TiS_3 nanoribbon photodetector illuminated with a red laser. (b) Transfer curve (V_b = 500 mV) for a TiS_3 nanoribbon photodetector in dark conductions (black curve) and upon illumination (green curve). Inset shows the current voltage characteristics at V_g = -40 V for the same laser excitation. (c) Current-voltage characteristics at $V_g = -40$ V in dark (black solid line) and under 640 nm excitation for increasing laser powers up to 3 mW. (d) Log-log plot of the responsivity (R) as a function of excitation power (λ = 640 nm). (e) Photocurrent as a function of illumination wavelength. (f) Photocurrent response using a 10 Hz mechanically modulated optical excitation (λ = 640 nm, P = 500 μW).]

J. O. Island, A. J. Molina-Mendoza, M. Barawi, R. Biele, E. Flores, J. M. Clamagirand, J. R. Ares, C. Sanchez, H. S. J. van der Zant1, R. D'Agosta, I. J.Ferrer, and A. Castellanos-Gomez,," 2D Mater. 4, 022003 (2017).

Temperature variation of photoconductivity, δσ, in TiS_3

$\delta\sigma \equiv \sigma_{light} - \sigma_{dark}$

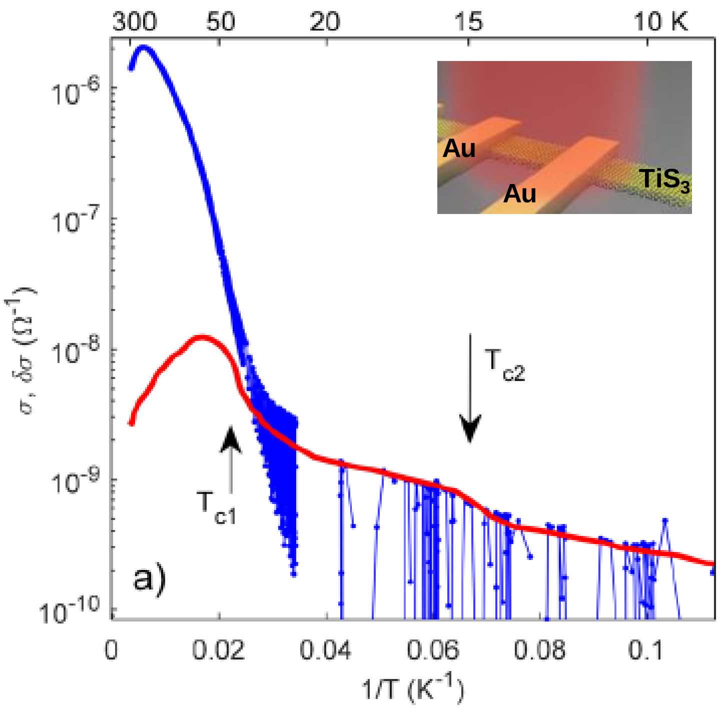

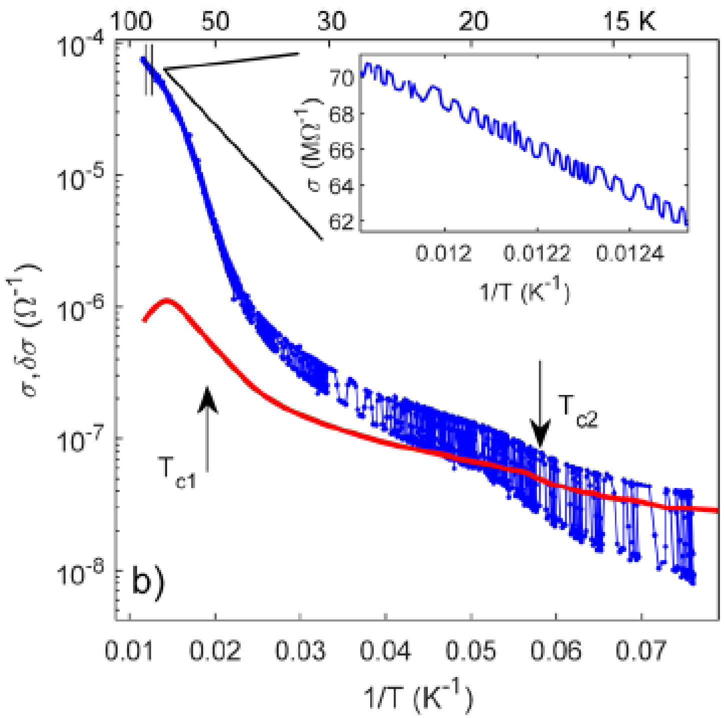

a) The $\sigma_{light/dark}(T)$ record for sample No 1 (the blue lines and points) and **δ**$\sigma(T)$ (the red line). b) Similar curves for sample No 2. The arrows mark the temperatures of the maxima of $-d\ln(\sigma)/d(1/T)$. The dimensions of sample No 1: 600 × 5.4 × 1.2 μm^3; of sample No 2: 250 × 50 × 2.5 μm^3. The inset to panel b) shows an enhanced fragment of $\sigma_{light/dark}(T)$ in the temperature interval of 80-84.5 K, indicated with two vertical bars in the main panel. λ=940 nm.

I.G. Gorlova, S.A. Nikonov, S.G. Zybtsev, V.Ya. Pokrovskii and A.N. Titov, Appl. Phys. Lett. ***120*** *(2022) 153102.*

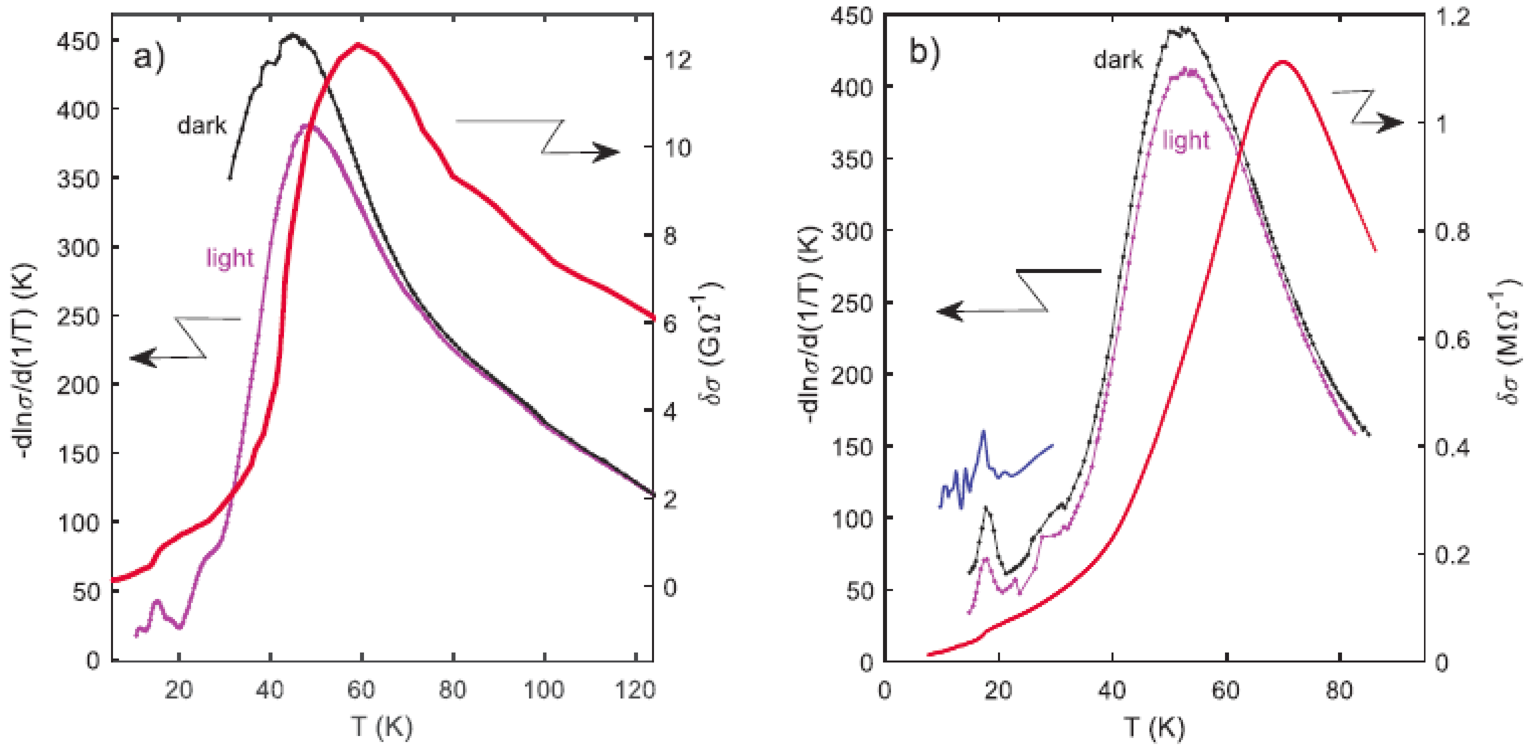

a) Temperature dependences of photoconductivity, $\delta\sigma(T)$, (red curve, the right scale) together with the logarithmic derivatives (the left scale) of σ_{light} (magenta) and σ_{dark} (black) for sample No 1. b) Similar curves for sample No 2. In addition, $-d\ln(\delta\sigma)/d(1/T)$ is shown (in blue) in the range of 10-30 K. The curve is shifted vertically by 100 K.

I.G. Gorlova, S.A. Nikonov, S.G. Zybtsev, V.Ya. Pokrovskii and A.N. Titov, Appl. Phys. Lett. ***120*** *(2022) 153102.*

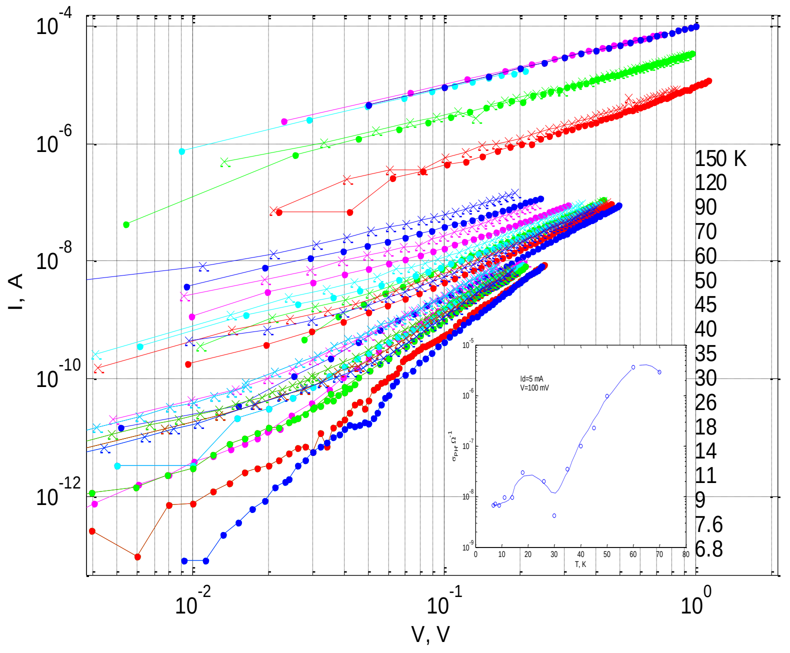

Current-voltage characteristics of TiS_3 in dark conditions. (•) and upon illumination (×) at different temperatures (different colors). λ=940 nm.
Insert: temperature dependence of photoconductivity at V=0.1 V.

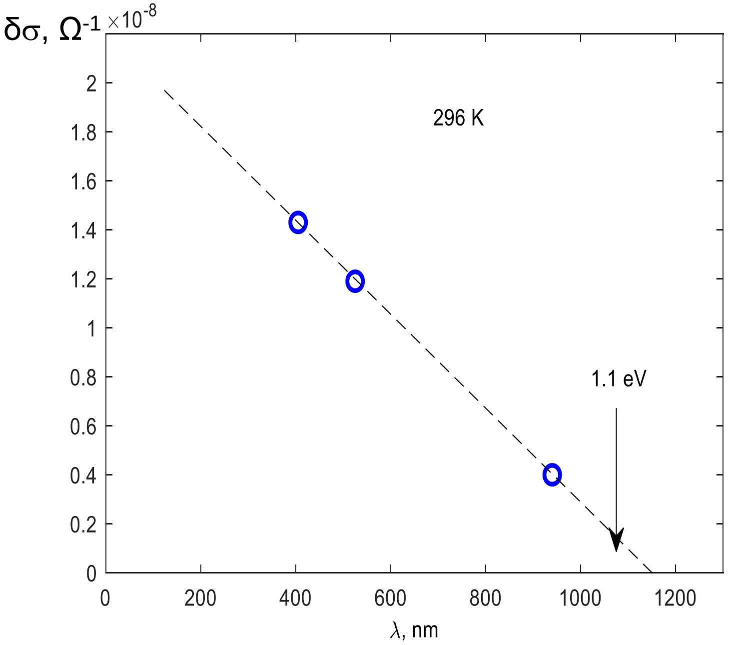

Photocoductivity as a function of illumination wavelength. Linearly extrapolating (dashed line) δσ vs. λ gives a rough estimate of the bandgap energy of 1.07 eV.

Photoconductivity in TiS_3 and CDW conductors

TiS_3

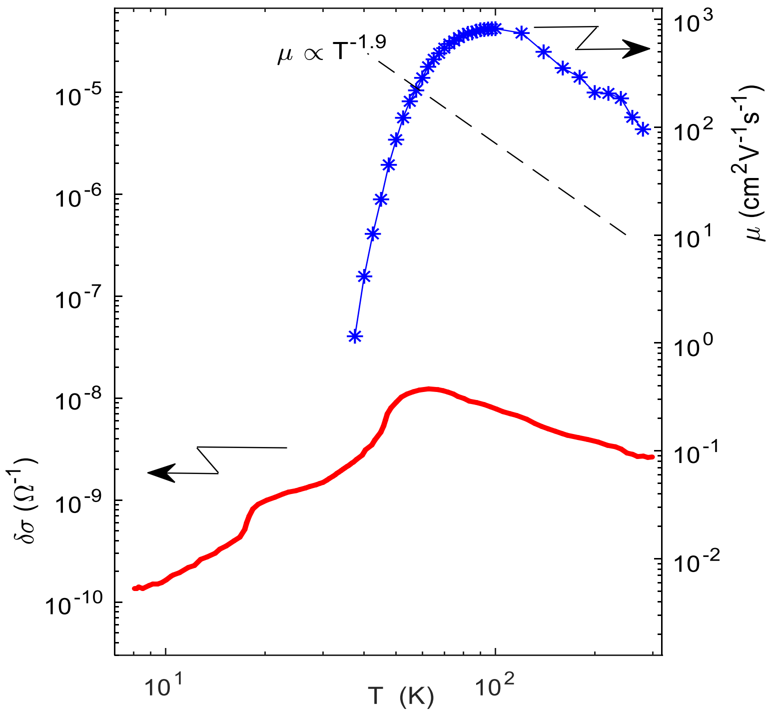

Temperature dependences of the photoconductivity (— the left scale) and Hall mobility of the electrons (-✱- the right scale)

I.G. Gorlova, S.A. Nikonov, S.G. Zybtsev, V.Ya. Pokrovskii and A.N. Titov, Appl. Phys. Lett. ***120*** *(2022) 153102.*

o-TaS_3

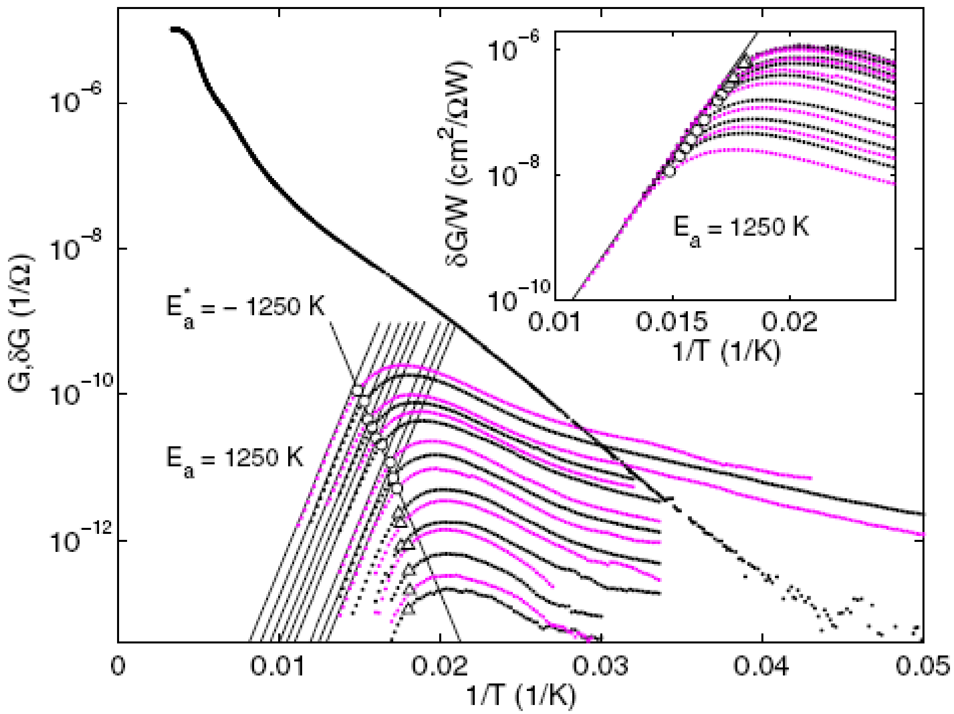

Temperature variation of the linear conductance of *o*-TaS_3 in the dark (upper curve). Set of curves shows temperature dependencies of ac photoconduction measured at different light intensities.

S.V. Zaitsev-Zotov and V. E. Minakova, Phys. Rev. Lett. ***97****, 266404 (2006).*

Relaxation of photoconductivity

TiS_3

o-TaS_3

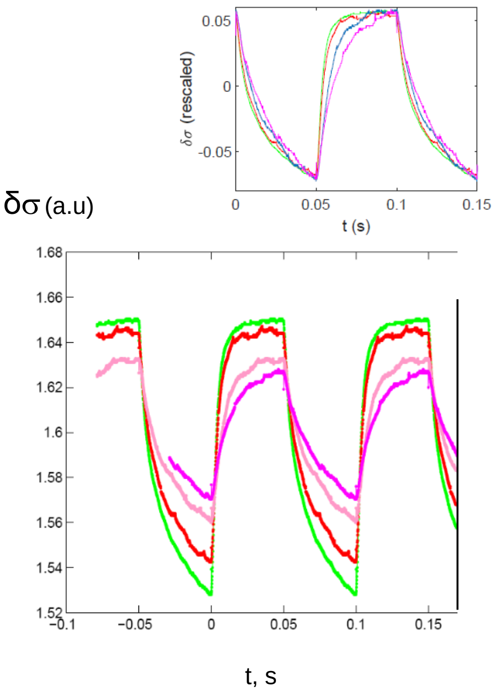

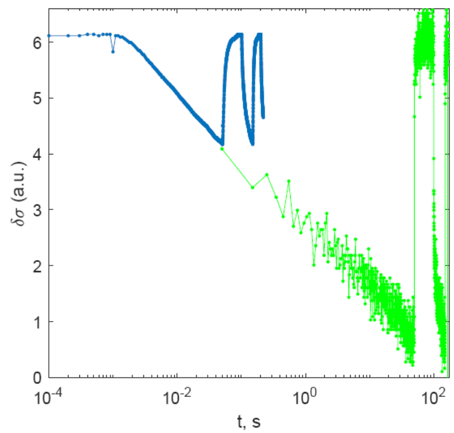

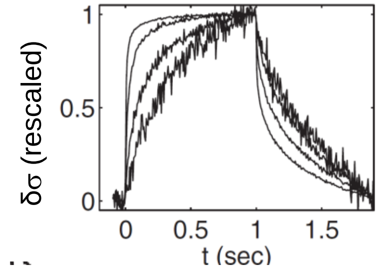

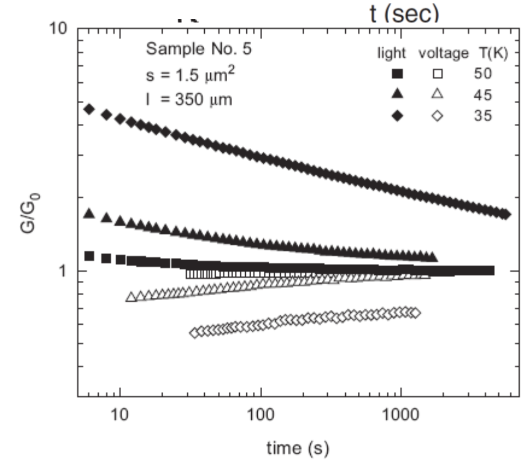

Fig. 6. Relaxation of metastable states produced by application of the voltage pulse (open symbols) and a light pulse (close symbols) in *o*-TaS_3 sample. All the curves are normalized by the "equilibrium conduction" G_0 obtained after cooling back from $T = 120$ K to remove "prehistory" effect. Data of Ref. [3].

Photoresponse under rectangular light pulses. λ=405 (-), 525 (-), 650 (-), 940 (-) нм, *T*=100 K. The curves are shifted vertically.

Relaxation of photoconductivity vs. log *t*. Two relaxation curves measured on different time scales are fitted and matched.

*S.V. Zaitsev-Zotov and V. E. Minakova, Phys. Rev. Lett. **97**, 266404 (2006).*

*S.V. Zaitsev-Zotov, V.E. Minakova, V.F. Nasretdinova, S.G. Zybtsev, Physica B **407** 1868 (2012)*

The estimates based on the values of δσ give the recombination time ~20 μs at 300 K. But the logarithmic relaxation suggests a wide distribution of relaxation times.

CONCLUSIONS

Photoconductivity, δσ, of the TiS_3 whiskers is studied in a wide temperature range covering the two suggested electronic phase transitions into CDW-like states.

Above ~100 K, TiS_3 behaves as a semiconductor, where electron-hole pairs are excited across the gap, while the recombination goes through transitions of the excited electrons to a donor level with a long lifetime.

The features in δσ(*T*) observed near 60K and near 17K can be attributed to condensation of the photo-excited carriers into a collective state.

But

Temperature variation of photoconductivity in TiS_3 is strikingly different from δσ(*T*) of the known quasi one-dimensional conductors with charge-density waves.

Possible mechanisms of magnetoresistance in TiS_3

Negative MR in transverse (out-of plane) fields, *B*||*c*

is observed in layered conductors with charge or antiferromagnetic ordering and is explained by localization induced by defects of different kind. E.g.:

$(DMtTSF)_2X$, X= BF_4, ClO_4, ReO_4. AF ordering**.** 2D weak localization induced by disorder in the anion lattice.
J. P. Ulmet et al., Phys. Rev. B ***38*** *7782 (1988).*

α-$(BEDT\text{-}TTF)_2I_3$. Ferroelectric CO phase transition. 2D weak localization induced by disorder in I layers.
T. Ivek et al., PRB 96 (2017) 075141

***o*-TaS_3** CDW. Delocalization of quantum interference of CDW loop formed in domain structure.
Katsuhiko Inagaki et al., Phys. Rev. B ***93****, 075423 (2016)*

Positive MR in parallel (in-plane) fields, *B*||*I*||*b*, *B*||a

is observed in 2D interacting low-density carrier ($n\sim10^{11}$ cm^{-2}) electron systems, 2D EG. **Si-MOS structures**.

Explanations:
Zeeman spin-splitting. *V. T. Dolgopolov and A. V. Gold, JETP Lett.* ***71****, 27 (2000).*

Both the spin and Coulomb interaction effects *V. M. Pudalov et al., JETP Lett.* ***65****, 932 (1997)*

The two parallel dissipation channels : scattering of the electrons by impurities in 2D Fermi liquid and Coulomb scattering of electrons by the collective localized states (spin droplets). *L. A. Morgun et al., Phys.Rev.B* ***93****, 235145 (2016)*

Intermediate phase between the Fermi-liquid and the Wigner crystal phases. *B. Spivak, Phys.Rev.B* ***67****, 125205 (2003)*

Samples

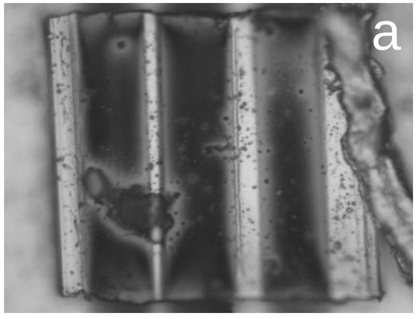

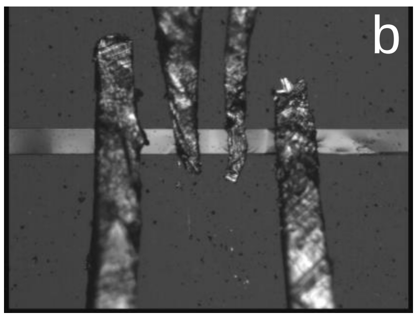

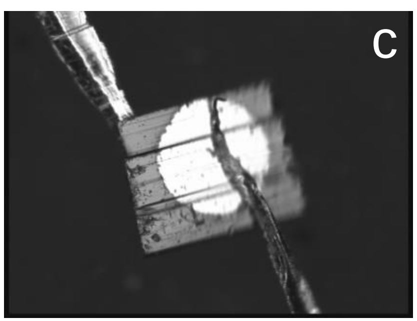

The TiS_3 whiskers with electrical contacts. The current flows along *a*- axis (a), *b*- axis (b), *c*- axis (c)

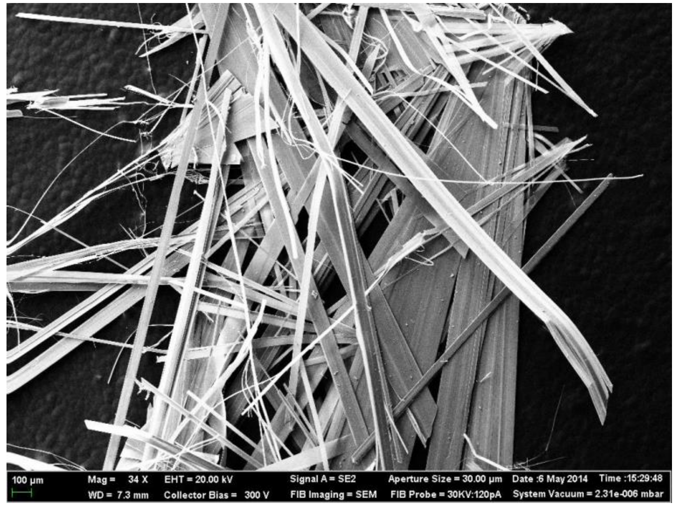

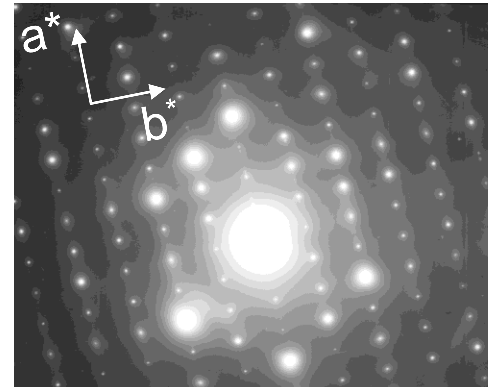

The diffraction patterns of the TiS_3 whisker at 285 K
HVEM JEM-1000

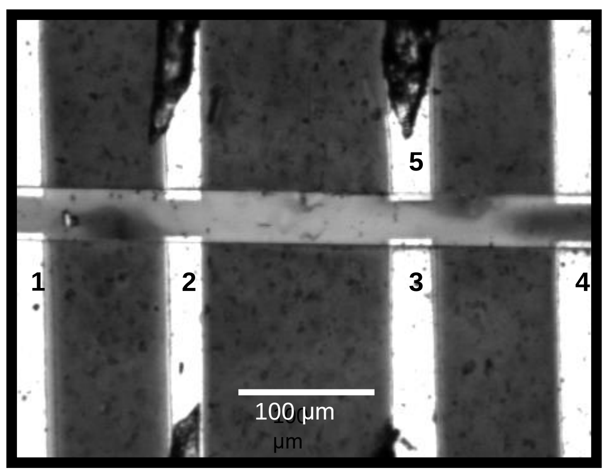

TiS_3 whisker (the gray stripe in the middle) with 8 Au contacts prepared for R_{xy} and R_{xx} measurements.

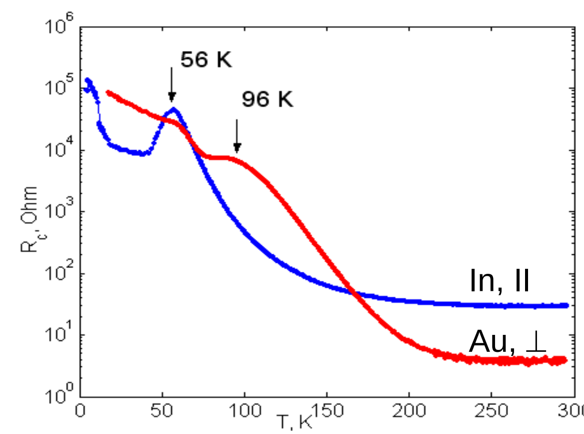

The temperature dependencies of the contact resistance to TiS_3 whiskers. Contact resistance at 300 K was ~ 10^{-6} Ohm x cm^2.

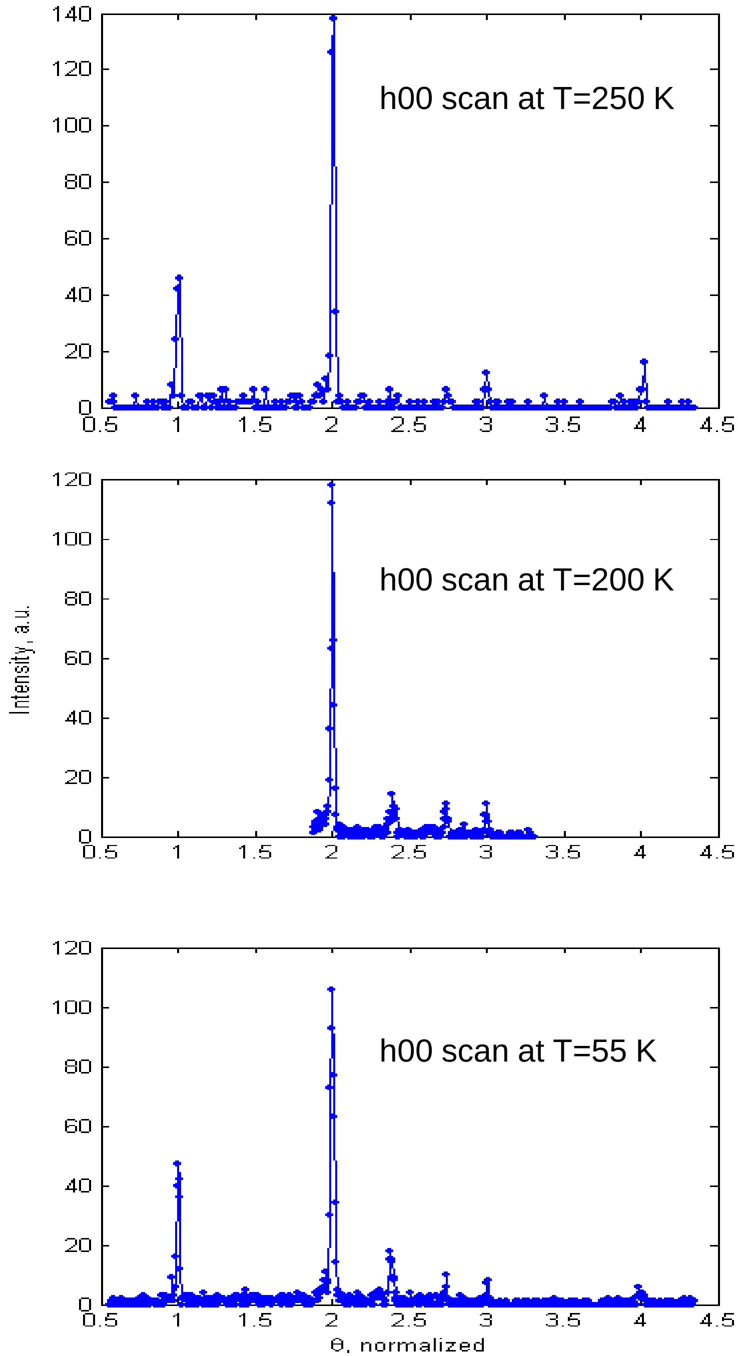

X-ray study of TiS_3 whiskers at different temperatures.

Scans along *a*-axis.

Shubnikov Institute of Crystallography of RAS

Low-temperature four-circle diffractometer **Huber 5042**

Mo-anode

Non-commensurate superstructure

along the ***a*** **-** *axis* with the period ≈ 12,72 Å**.**

I.G. Gorlova, S.G. Zybtsev, V.Ya. Pokrovskii, N.B. Bolotina, I.A. Verin and A.N. Titov, Physica B ***407****, 1707 (2012).*

Diffraction patterns in the [010] pole

synchrotron radiation

ESRF, CCD – diffractometer Xcalibur, Grenoble, France.

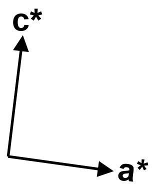

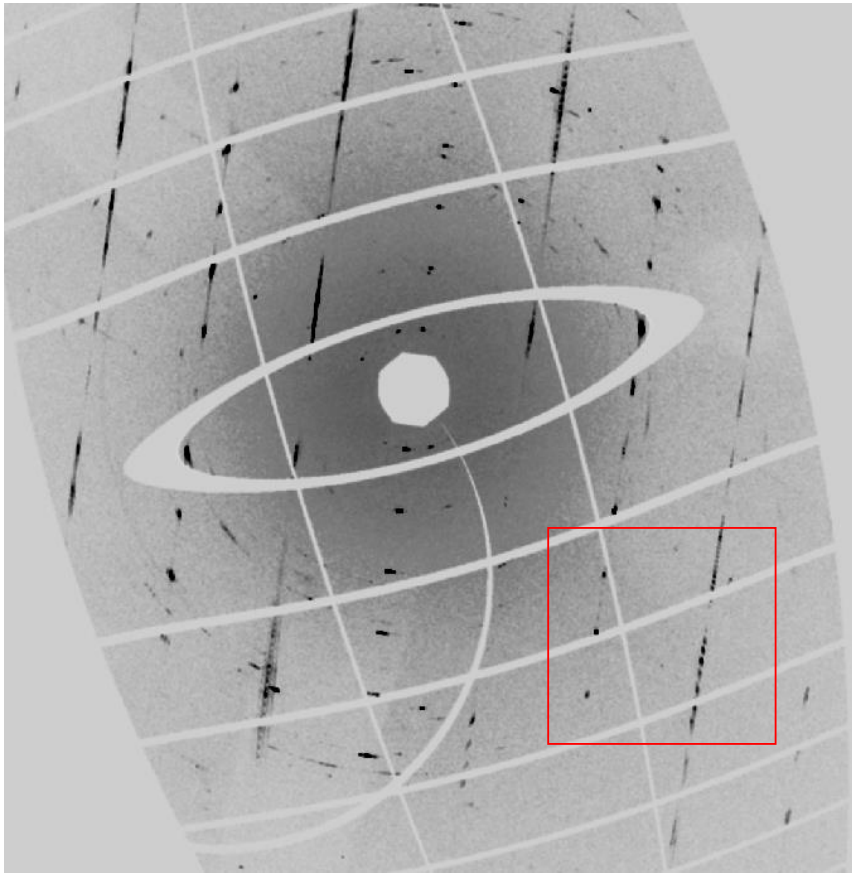

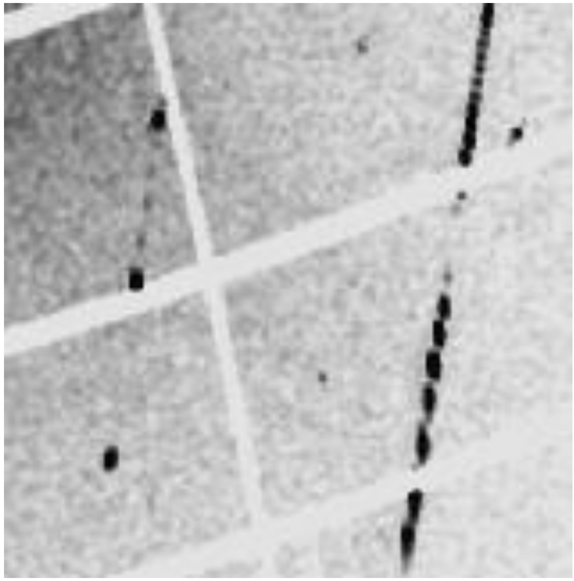

T =300 K

***ac* – plane** (h0l)

Non-commensurate superstructure

along the ***c*** **-** *axis* with the period ≈ 49Å

q ≈[0, 0, 0.18]

A. Arakcheeva, N. Bolotina, I. Gorlova, Ph. Pattison, to be published.

2D Coulomb interaction within the conductive layers.

Power law behavior of layered charge-ordered organic crystals **θ-(BEDT-TTF)$_2$*M*Zn(SCN)$_4$ (*M*=Cs,Rb)**

Y. Takahide, M. Kimata, K. Hazama,et al.,, Phys. Rev. B 81, 235110 (2010)

and the Mott insulator **κ-(BEDT-TTF)$_2$Cu[N(CN)$_2$]Cl**

Y. Takahide, M. Kimata, K. Kodama, et.al.,Phys. Rev. B 84, 035129 (2011)

TAKAHIDE *et al.* PHYSICAL REVIEW B **81**, 235110 (2010)

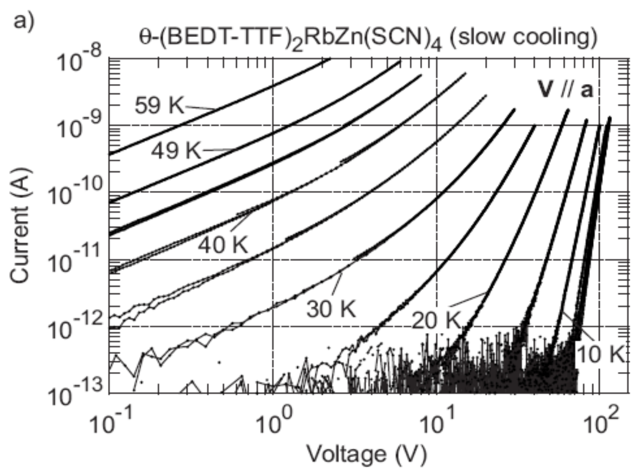

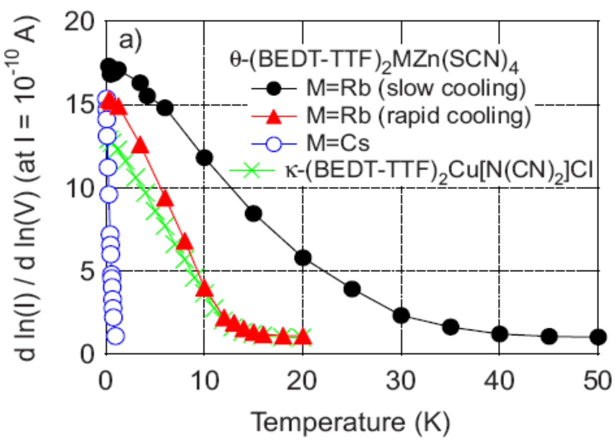

Electric field-induced unbinding of electron-hole pairs.

Y. Takahide, T. Konoike, et al., Phys.Rev.Lett. ***96,*** *136602 (2006)*

$U = A \ln(r)$, $r_0 \propto V^{-1}$,

$R \propto n \propto \exp[-U(r_0)/T)] \propto r_0^{-a(T)} \propto V^{(a)}$,

где $a(T)=A/T$

Theory:

See, e.g., R.Fazio, G Schön Phys.Rev.B ***43*** *, 5307 (1991)*

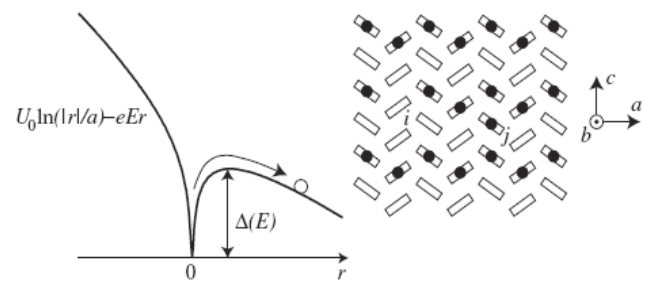

FIG. 3. Left: Schematic drawing of a particle escaping from a tilted logarithmic potential due to thermal activation. Right: Charge-ordered state with an excitation of an electron-hole pair. The boxes represent ET molecules and the dots represent holes.

Структуры типа полевого транзистора на основе вискеров TiS3

Образцы

Синтез

ИФМ УрО РАН (Екатеринбург)

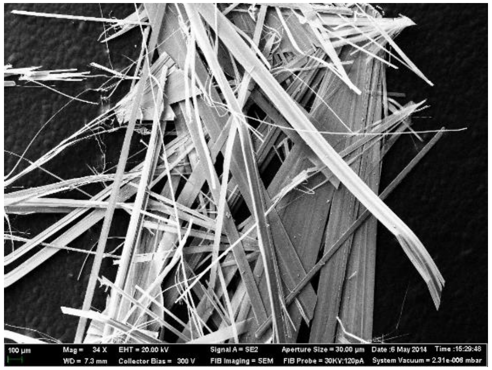

Схема измерений

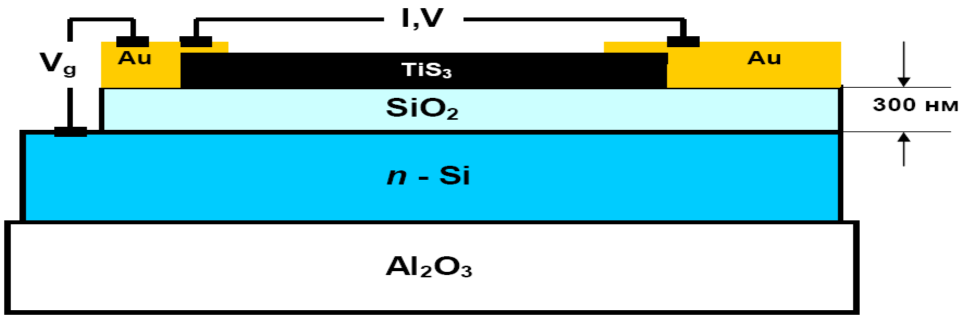

Фотография микроструктуры

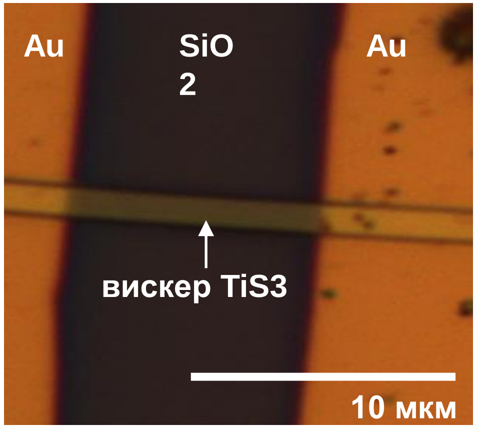

Размеры вискера:
L = 9.36мкм, w = 1.27 мкм, t≈ 0.4 мкм

Изображение микроструктуры в РЭМ

Carl Zeiss Neon 40 EsB (CrossBeam).

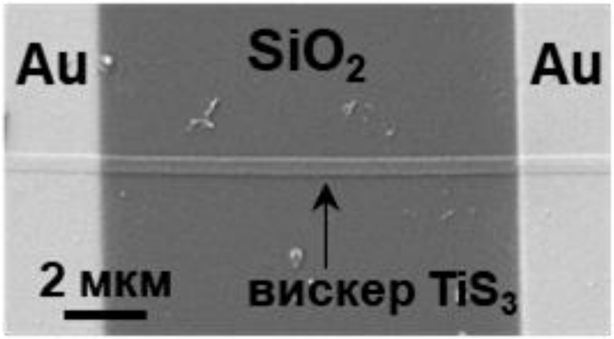

Размеры вискера:
L = 9.5мкм, w = 0.39 мкм, t≈ 0.05 мкм